Modifications to Transonic Flow Codes for Unsteady Perturbations Around an Experimental Mean

L. C. Rodman* and D. Nixon†
Nielsen Engineering and Research, Inc., Mountain View, California
and
L. J. Huttsell‡
Air Force Wright Aeronautical Laboratories, Wright-Patterson Air Force Base, Ohio

The transonic small-disturbance equation is often used to compute unsteady transonic flow over a wing. However, as the equation assumes isentropic flow, it is inaccurate for strong shock waves. The inaccuracy is mostly seen as an incorrect time-averaged shock location, whereas the prediction of the time-accurate fluctuation about the mean is satisfactory. The time-averaged solution may be corrected using steady-state experimental data, but first the solution must be written in a strained coordinate system so that the shock movement, and thus the nonlinearities, are removed. This technique has been used in both two- and three-dimensional calculations, and has been shown to correct satisfactorily the time-accurate shock locations. Slight errors in the corrected pressure distributions may be attributed to scatter in the experimental data and to the interpolation between sparse data points.

Nomenclature

C_p = unsteady pressure coefficient
C_{p_s} = steady pressure coefficient
C_{p_1} = perturbation pressure coefficient
C_{p_E} = experimental steady pressure coefficient
C_{p_T} = total pressure coefficient
c = airfoil or local wing chord
k = reduced frequency (based on chord)
M_∞ = freestream Mach number
x,y,z = chordwise, spanwise, and normal Cartesian coordinates
x',y' = strained coordinates
α_0 = mean angle of attack
α_1 = amplitude of pitching oscillation
β_0 = mean flap angle
β_1 = amplitude of flap oscillation
γ = ratio of specific heats
ρ = density
ϕ = perturbation velocity potential
ϕ_0 = steady base component of the potential
ϕ_1 = unsteady perturbation velocity potential

Introduction

THE problem of aeroelasticity has existed in airplane design since flying machines were first built, and, consequently, a considerable body of knowledge on the subject exists. However, there are some areas where aeroelastic predictions are not as accurate as they should be, and one of these regimes is at transonic speeds. The problem has been compounded in recent years by the advent of active control technology that allows an airplane to fly closer to its aeroelastic limit than previously; this means that better accuracy is required of a prediction method, since the margin between safe flight and flutter is greatly reduced.

The only practical means of predicting the unsteady aerodynamic effects is to solve the transonic small-disturbance (TSD) equations. Although other methods exist, such as those based on the full potential or Euler equations, these are still in the development phase. The original version of the TSD equation[1] is a potential equation linear in all directions except the streamwise direction, where a second-order term is included to model shock waves normal to the freestream. Although adequate for two-dimensional flows or flows over rectangular wings, it is not adequate for swept wings. The TSD equation can be extended[2] to give adequate results for swept wings by the addition of nonlinear terms in the spanwise direction; this adds to the complexity of the equation.

The work reported in Refs. 1 and 2 is concerned with steady flow. The formulation can be extended to unsteady flow, and a series of codes—the LTRAN2 code initiated by Ballhaus and Goorjian[3] and the XTRAN3 code initiated by Borland et al.[4]—are available to solve the general-frequency unsteady TSD equation. One problem with the XTRAN3S code is that the steady-state version of the equation does not model adequately the real flow as measured in an experiment. Thus, even if the unsteady part of the calculation is adequate, the unsteady perturbation is about an inaccurate mean and, thus, the overall solution is in error. It is suggested that if the unsteady calculation procedure could use experimental data as a mean, then the overall accuracy of the predictions could be improved considerably. A procedure for achieving this goal is given in the present work.

A possible means of incorporating experimental values into the solution would be to use the value of the surface pressure as a boundary condition and to derive an equivalent potential model of the wing. This modified wing could then be used in the unsteady calculation. However, there are some constraints[5] on the use of inverse design methods for compressible flows that could limit the usefulness of the idea.

Another method of incorporating experimental values into the XTRAN3S code would be to use experimentally determined velocity at all grid points in the flowfield and then perform an unsteady perturbation around these values. This is a viable approach, but does require the development of a method to solve the resulting unsteady perturbation equation,

Presented as Paper 89-0447 at the AIAA 27th Aerospace Sciences Meeting, Reno, NV, Jan. 9–12, 1989; received Jan. 23, 1989; revision received March 23, 1989. This paper is declared a work of the U.S. Government and is not subject to copyright protection in the United States.

*Research Scientist. Member AIAA.
†President.
‡Aerospace Engineer. Associate Fellow AIAA.

which would involve the development of a treatment for moving shock waves. This is a major, and possibly unnecessary, undertaking.

The method presented in this report has been developed to achieve the same end as those techniques noted earlier, but with a minimum of cost and the maximum use of existing and proven technology. The technique simply requires that the steady part of the XTRAN3S solution be subtracted from the overall solution and replaced by the experimental data. The crucial need to treat different shock-wave locations is met by using a strained coordinate system.[6,7] This is described in later sections. The method does not alter the algorithm or the grid used in XTRAN3S, since it acts as a post/processor on the pressure. This allows the use of any code that will solve the unsteady TSD equation.

Technical Approach

The general-frequency TSD equation is given as

$$(A\phi_t + B\phi_x)_t = (E\phi_x + F\phi_x^2 + G\phi_y^2)_x + (\phi_y + H\phi_x\phi_y)_y + \phi_{zz} \quad (1)$$

where

$$A = M_\infty^2 k^2$$

$$B = 2M_\infty^2 k$$

$$E = 1 - M_\infty^2$$

$$F = -[3 + (\gamma - 2)M_\infty^2]M_\infty^2/2$$

$$G = -M_\infty^2/2$$

$$H = -M_\infty^2 \quad (2)$$

The tangency boundary condition for Eq. (1) is

$$\phi_z(x,y,\pm 0,t) = f_x^\pm(x,y,t) + f_t^\pm(x,y,t) \quad (3)$$

where

$$z = f^\pm(x,y,t) \quad (4)$$

denotes the (moving) wing surface; the superscripts + and − denote the upper and lower surfaces, respectively.

It is shown in Ref. 6 that an equation similar to Eq. (1) can be decoupled into a steady base solution ϕ_0 and a uniformly valid unsteady perturbation ϕ_1, if a strained coordinate system (x',y',z) is used. The complete base and perturbation equations are as follows.

The base equation is

$$(E\phi_{0_{x'}} + F\phi_{0_{x'}}^2 + G\phi_{0_{y'}}^2)_{x'} + (\phi_{0_{y'}} + H\phi_{0_{x'}}\phi_{0_{y'}})_{y'} + \phi_{0_{zz}} = 0 \quad (5)$$

with the boundary condition

$$\phi_{0_z}(x',y',\pm 0) = f_{0_{x'}}^\pm(x',y') \quad (6)$$

where

$$z = f_0^\pm(x',y')$$

denotes the steady wing geometry.

The perturbation equation is

$$(A\phi_{1_t} + B\phi_{1_{x'}})_t = (E\phi_{1_{x'}} + 2F\phi_{0_{x'}}\phi_{1_{x'}} + 2G\phi_{1_{y'}}\phi_{0_{y'}} + F\phi_{1_{x'}}^2 + G\phi_{1_{y'}}^2)_{x'} + [\phi_{1_{y'}} + H(\phi_{1_{y'}}\phi_{0_{y'}} + \phi_{1_{y'}}\phi_{0_{x'}}) + H\phi_{1_{x'}}\phi_{1_{y'}}]_{y'} + \phi_{1zz} + S_1(\phi_0,\phi_1) \quad (7)$$

with the tangency boundary condition

$$\phi_{1_z}(x',y',\pm 0,t) = f_{1_{x'}}^\pm(x',y',t) + f_{1_t}^\pm(x',y',t) + \bar{S}_1(f_0) \quad (8)$$

where

$$z = f_1^\pm(x',y',t)$$

denotes the unsteady motion of the wing surface.

In Eqs. (5–8), $\phi(x,y,z,t)$ is given by

$$\phi(x,y,z,t) = \phi_0(x',y',z) + \phi_1(x',y',z,t) \quad (9)$$

The coordinates are related by

$$x = x' + \bar{x}_1(x',y',t) \quad (10)$$

$$y = y' + \bar{y}_1(y',t) \quad (11)$$

where $\bar{x}_1(x',y',t)$ and $\bar{y}_1(y',t)$ are specified straining functions.

In Eqs. (7) and (8), $S_1(\phi_0,\phi_1)$ and $S_1(f_0)$ represent the additional terms caused by the coordinate straining. If the coordinate straining is zero, these terms vanish. Equations (7) and (8) are exact; no terms have been neglected. The new coordinates are chosen such that in the (x',y',z,t) system the shock waves do not change location with time. This means that ϕ_1 is the same order of magnitude throughout.[6]

In general, ϕ_1 is a function of ϕ_0, $\bar{x}_1$, and $\bar{y}_1$; the latter terms contain the information about the shock motion. It is interesting to speculate whether ϕ_1 is a strong or a weak function of ϕ_0.

Before computers were generally available, it was common to simplify the governing equations so that an analytic solution might be obtained. The most common of these simplifications leads to linear theory that linearizes the flow about freestream conditions. For example, if the ϕ_0 terms are neglected in Eq. (7), then the resulting equation is the linear potential equation for ϕ_1 and is independent of ϕ_0. It was found in these linear theories that the perturbation about freestream could be quite large, around 20% or 30%, and still give adequate answers.

Consider now the equation for density ρ in an inviscid fluid, given by

$$\frac{\rho}{\rho_\infty} = \left[(1 + \frac{\gamma-1}{2}M_\infty^2)/(1 + \frac{\gamma-1}{2}M^2)\right]^{1/\gamma-1} \quad (12)$$

where M is the local Mach number, and ρ_∞ is a freestream value of ρ. An inviscid flow model will not be adequate if M is greater than about 1.3 because of flow separation. If M_∞ is taken to be 0.8 and M is taken to be 1.2, a relatively large value for potential flow conditions,

$$\frac{\rho}{\rho_\infty} = 0.718 = 1 - 0.282 \quad (13)$$

In other words, the perturbation for transonic flow is the same order of magnitude as for subsonic flow, and it could be expected that, apart from the shock waves, transonic flow could be described by a linear equation. In Eq. (7), the shock waves are fixed for all time in the (x',y',z,t) coordinate equation, and ϕ_1 is a perturbation about ϕ_0 and the freestream; the shock motion information is contained in the straining terms. Consequently, it can be argued that ϕ_1 is a weak function of ϕ_0 and is not changed significantly if ϕ_0 is replaced by some neighboring value $\bar{\phi}_0$, which could be an experimentally determined function. Thus, it is suggested that to a first approximation ϕ_1 is not affected if ϕ_0 is replaced by an experimental value $\bar{\phi}_0$, provided the strained coordinate system is now chosen such that shock-wave locations are invariant in the system for the experimental and calculated values of ϕ_0, $\bar{\phi}_0$, and ϕ_1.

Let the coordinate straining functions of Eqs. (10) and (11) be written as

$$x = x' + \sum_{k=1}^{2} \delta x_{s_k}(y',t)x_{1_k}(x',y') \quad (14)$$

$$y = y' + \delta y_s(t)y_1(y') \quad (15)$$

where $\delta x_{s_k}(y',t)$ denotes a change in the kth shock location at spanwise station y' at time t, and $\delta y_s(t)$ denotes a change in a spanwise shock termination point at time t; it is assumed that there are a maximum of two shocks on the wing surface. If the steady, calculated surface pressure distribution is denoted by $C_{p_s}(x,y)$ and the unsteady values denoted by $C_p(x,y,t)$, then the correct value of the perturbations in pressure C_{p_1} due to motion is given by

$$C_{p_1}(x',y',t) = C_p(\bar{x},\bar{y},t) - C_{p_s}(x',y') \tag{16}$$

where

$$\bar{x} = x' + \sum_{k=1}^{2} \delta x_{s_k}(y',t) x_{1_k}(x',y') \tag{17a}$$

$$\bar{y} = y' + \delta y_s(t) y_1(y') \tag{17b}$$

If an experimentally determined steady flow pressure coefficient is given by $C_{p_E}(x,y)$, then the strained coordinates must be chosen so that C_{p_E} rather than C_{p_s} is the base. Thus, total pressure $C_{p_T}(x,y,t)$ is given by

$$C_{p_T}(x,y,t) = C_{p_E}(x',y') + C_{p_1}(x',y',t) \tag{18}$$

$$x = x' + \sum_{k=1}^{2} [\delta x_{s_k}(y',t) + \delta x_{s_{E_k}}(y')] x_{0_k}(x',y') \tag{19a}$$

$$y = y' + [\delta y_s(t) + \delta_{y_{s_E}}] y_1(y') \tag{19b}$$

where $\delta x_{s_{E_k}}(y)$ is the change in the kth shock location at y', and δy_E the change in a shock termination point between experimental and calculated steady pressures.

It should be noted that apart from the hypothesis that $\phi_1(x',y',z,t)$ and, consequently, $C_{p_1}(x',y',t)$ are weak functions of $\phi_0(x',y',z,t)$, if the strained coordinate system is chosen correctly, there are no further assumptions regarding the magnitude of the perturbation quantities C_{p_1}, ϕ_1, etc.

This analysis is only valid[6] if shock waves are not generated or destroyed during the motion. In the present context, this restriction means that the shock pattern in the steady, unsteady, and experimental data must be similar.

Straining Function

It is shown in Ref. 8 that in the strained coordinate method the precise form of the straining functions is unimportant. In the present case, the following functions are used; it is assumed that there are two shock waves, at points x_A and x_B, at some spanwise station on the wing, and that one shock terminates at a point y_s along the span. The wing root is denoted by y_R and the wingtip by y_T:

$$\bar{x}_1(x',y') = \begin{cases} \delta x_A x'/x'_A, & 0 < x'_A \\ (\delta x_A - \delta x_B)(x' - x_A)/(x'_B - x'_A), & x'_A \le x' \le x'_B \\ -\delta x_B(x'-1)/(1-x'_B), & x'_B \le x' \le 1 \end{cases} \tag{20}$$

$$\bar{y}_1(y') = \begin{cases} \delta_{y_s}(y' - y'_R)/(y'_s + y'_R), & y'_R \le y' \le y'_s \\ \delta_{y_s}(y' - y'_T)/(y'_s - y'_T), & y'_s \le y' \le y'_T \end{cases} \tag{21}$$

Shock Identification

It is necessary to define whether a shock is present. The best way is to compute the shock geometry and to determine the location of the point where the pressure coefficient is equal to its critical value based on flow conditions normal to the shock. This is complicated, and in the present case the shock is taken to be the location of C_p^* based on freestream conditions. For highly swept wings, it may be advantageous to multiply the theoretical value of C_p^* by a small factor, for example, 1.10; this makes some allowance for swept shock waves.

Comparison with Experimental Data

In general, the data from unsteady transonic experiments is processed by Fourier transforms to give fundamental response and the various harmonics. In the present work, $C_{p_T}(x,y,t)$, given by Eq. (18), is decomposed into a Fourier series of the type

$$C_{p_T}(x_1,y_1,t) = \sum_{n=0}^{\infty} A_n(x,y) \exp(in\omega t) \tag{22}$$

where ω is the frequency of oscillation. The coefficient A_0 gives the mean (steady) value, and the real and imaginary parts of $A_1(x,y)$ give the familiar real and imaginary parts of C_{p_T}. The Fourier series device is used rather than the Fourier transform because the coefficients A_n, given by

$$A_n = \frac{1}{T}\int_0^T F(t) \exp(in\omega t)\, dt \tag{23}$$

where T is the period, involve running sums. This avoids the need to store data at each time step over a cycle, a massive undertaking for three-dimensional examples.

Two-Dimensional Results

Corrected results from the two-dimensional XTRAN2L code are presented here. Three test cases were run on a VAX 11/750, with the unsteady calculation covering four cycles of airfoil oscillation with 360 time steps per cycle. The three test cases are shown in Table 1. The first test case matches an

Table 1 Test cases for the two-dimensional pressure correction

Case	Airfoil	Mach no.	α_0	α_1	β_0	β_1	k
1	NACA 64A010	0.796	−0.21	0.51	0.0	0.0	0.101
2	NACA 64A006	0.875	0.00	0.0	0.0	1.0	0.235
3	NLR 7301	0.700	2.00	0.5	0.0	0.0	0.192

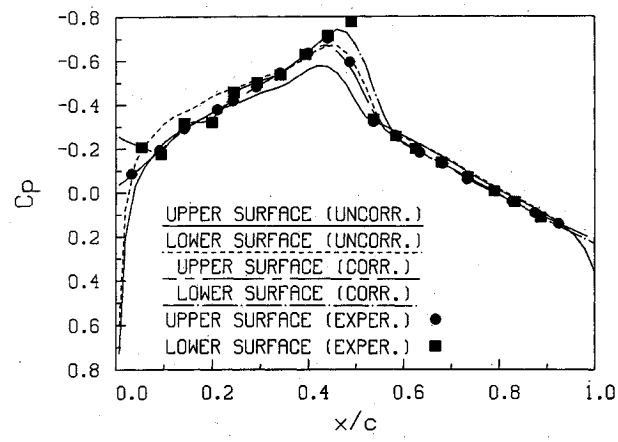

Fig. 1 Mean pressure distribution about a NACA 64A010 airfoil (case 1).

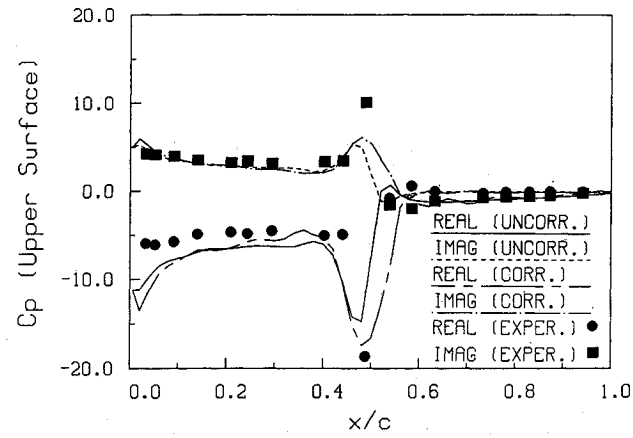

Fig. 2 Upper-surface unsteady pressure distribution about a NACA 64A010 airfoil (case 1).

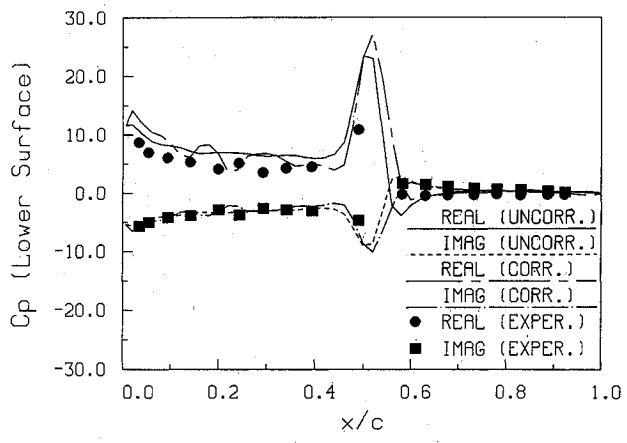

Fig. 3 Lower-surface unsteady pressure distribution about a NACA 64A010 airfoil (case 1).

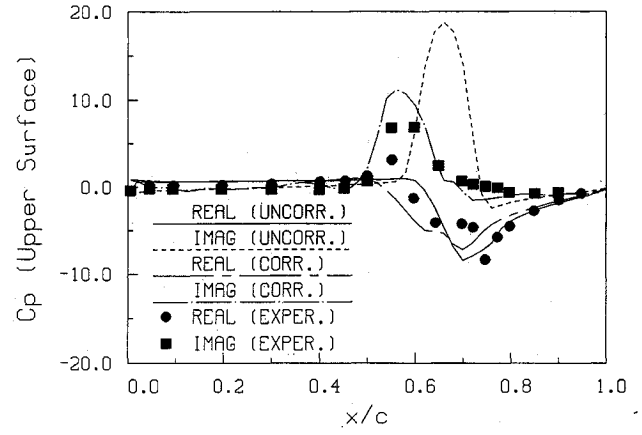

Fig. 5 Upper-surface unsteady pressure distribution about a NACA 64A006 airfoil (case 2).

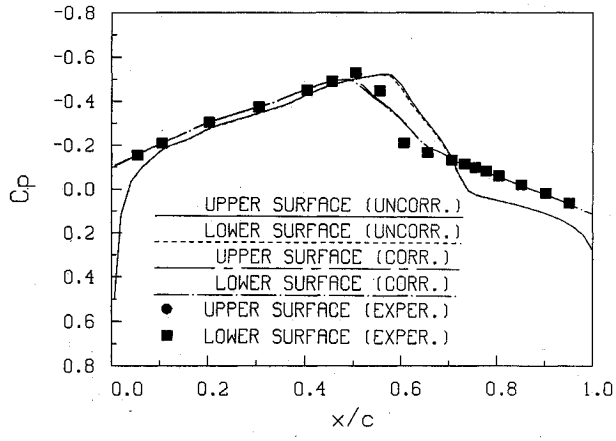

Fig. 4 Mean pressure distribution about a NACA 64A006 airfoil (case 2).

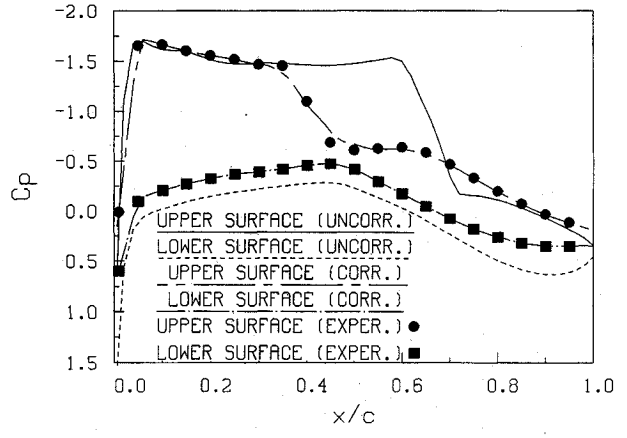

Fig. 6 Mean pressure distribution about an NLR 7301 airfoil (case 3).

experiment reported in Ref. 9, and the second and third cases use experimental data from Refs. 10 and 11, respectively.

In each case, a pressure correction is determined from the numerical steady-state pressure distribution and experimental results. This correction is applied at every time step during the unsteady calculation.

Figures 1-7 show the results from these calculations. For each case, results are plotted showing the time mean of the unsteady pressure distribution, and the upper and lower surface real and imaginary unsteady pressures. Both corrected and uncorrected numerical results are compared with experimental data.

The results for case 1 (NACA 64A010) are shown in Figs. 1-3. The time mean of the unsteady pressure distribution is compared with steady-state experimental pressures in Fig. 1. The effect of the correction is to increase the suction peak ahead of the shock to a value closer to the experimental level. The shock location was also moved rearward slightly. It is interesting to note that the corrected pressures do not have the positive pressure peak at the leading edge, since the correction is derived from extrapolated experimental pressures. A similar effect can be seen when scatter in the experimental results causes waviness in the corrected pressures.

Figures 2 and 3 show the unsteady results for the upper and lower surfaces. Again, the correction increases the magnitude of the real and imaginary pressure peaks and slightly moves the shock rearward. On the upper surface (Fig. 2), the correction provides a slight improvement in the comparison with experiment. On the lower surface, however, the peak pressures appear to be overestimated, although the sparseness of the experimental data points in the shock region makes it difficult to draw conclusions. The waviness in the corrected curves is again attributed to scatter in the data.

Figures 4 and 5 show results for the second case (NACA 64A006). The corrected mean pressure distribution provides a better match to the experimental data than does the uncorrected. The upper and lower surfaces overlay one another, since the flap is oscillating about zero angle of attack. The unsteady results (Fig. 5) show that the correction lowers the peak real and imaginary pressures and moves the shock wave forward. The general shape of the real part of the pressures in the shock region is also more accurately computed by the correction algorithm. Lower-surface unsteady results (not shown) are symmetric with upper-surface results.

The results for case 3 (NLR 7301) show the greatest discrepancy between the uncorrected numerical and experimental pressure distributions, and it is this case where the correction makes the most improvement. As shown in Fig. 6, the correction moves the shock position forward about 20% of the chord, which gives excellent agreement with experimental data. The corrected unsteady results (Fig. 7) for the upper surface show the shock in the proper position, and the real and imaginary pressure peaks have the correct magnitude. This is a large improvement over the uncorrected numerical results. The unsteady results for the lower surface are not shown, since there are no shock waves and thus no correction on that surface.

Three-Dimensional Results

The corrected XTRAN3S code was used to compute the unsteady pressures about an F-5 wing at a Mach number of 0.95 and zero mean angle of attack. Two cases were run on a Cray X-MP: one with a pitching frequency of 20 Hz and an amplitude of 0.523 deg (reduced frequency = 0.132), and the other with a pitching frequency of 40 Hz with an amplitude of

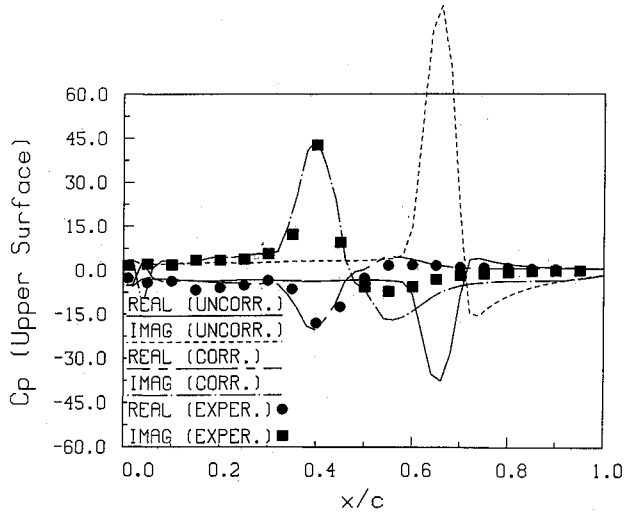

Fig. 7 Upper-surface unsteady pressure distribution about an NLR 7301 airfoil (case 3).

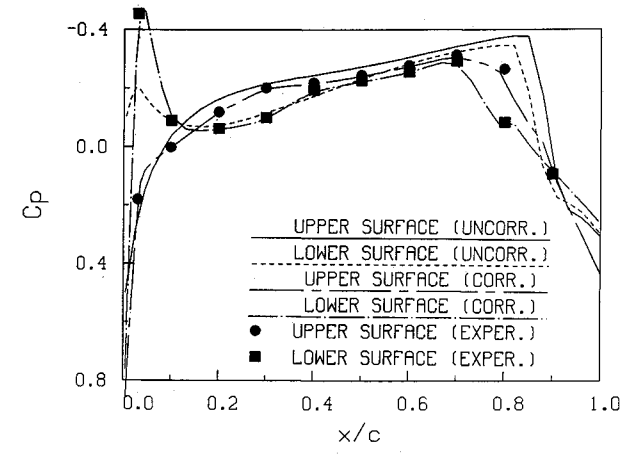

Fig. 8 Mean pressure distribution about the F-5 wing (34% span, 20 Hz).

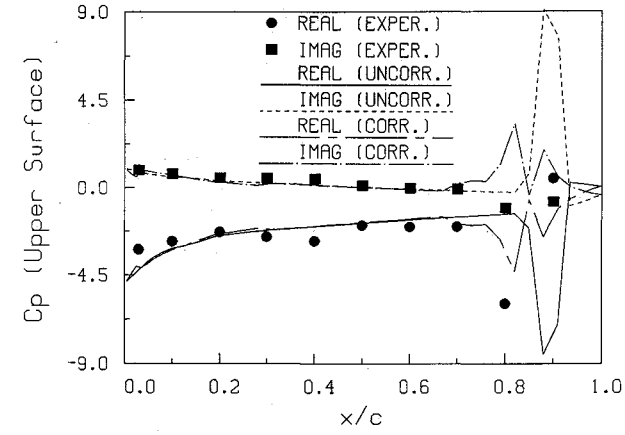

Fig. 9 Upper-surface unsteady pressure distribution about the F-5 wing (34% span, 20 Hz).

0.222 deg (reduced frequency = 0.264). These cases match experimental results reported in Ref. 12.

As with the two-dimensional cases, a pressure correction was applied at every time step. The results are shown in Figs. 8–19.

Figures 8–16 show the results for the 20-Hz case at spanwise locations = 34.2, 62.4, and 99.9% of span. Selected results at 34% span for the 40-Hz case are shown in Figs. 17–19. For each spanwise location, results are plotted showing the time mean of the unsteady pressure distribution, and the upper and

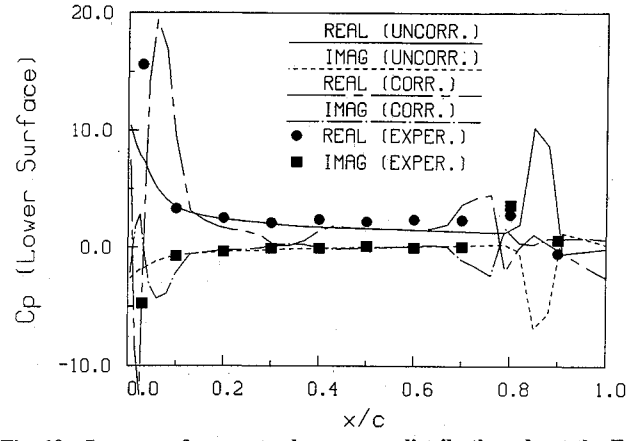

Fig. 10 Lower-surface unsteady pressure distribution about the F-5 wing (34% span, 20 Hz).

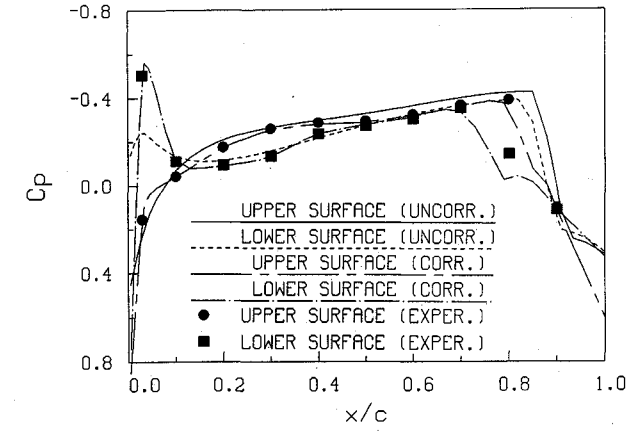

Fig. 11 Mean pressure distribution about the F-5 wing (62% span, 20 Hz).

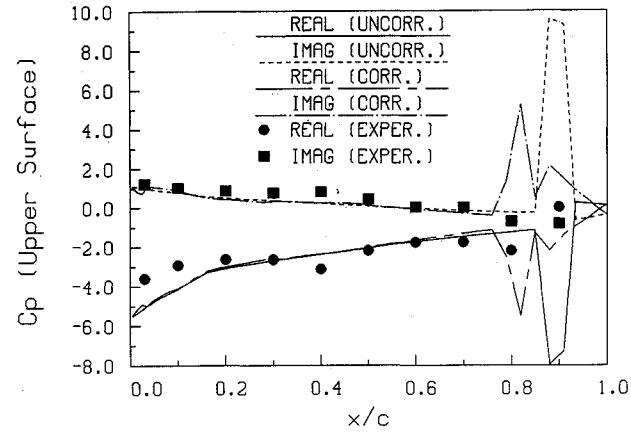

Fig. 12 Upper-surface unsteady pressure distribution about the F-5 wing (62% span, 20 Hz).

lower surface real and imaginary pressures. Both corrected and uncorrected numerical results are compared with experimental data.

In all cases, the pressure correction caused the mean trailing-edge shock location to move forward. This agreed with the experimental data. The leading-edge shock on the lower surface was also more accurately predicted with the corrected results. The corrected numerical trailing-edge shocks became spread out and slightly jagged compared with the uncorrected shocks. This was caused by the interpolation (both chordwise and spanwise) between sparse experimental data points used in the correction.

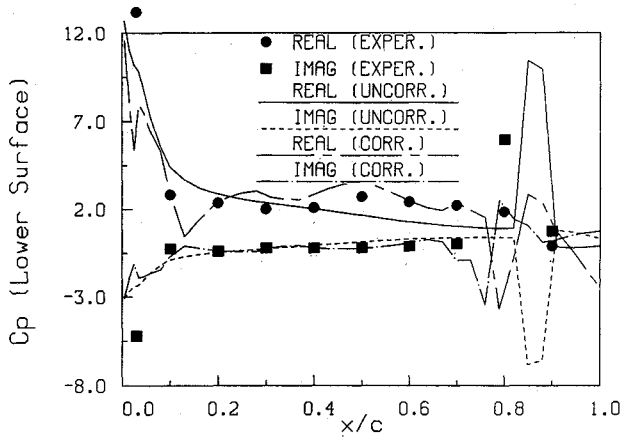

Fig. 13 Lower-surface unsteady pressure distribution about the F-5 wing (62% span, 20 Hz).

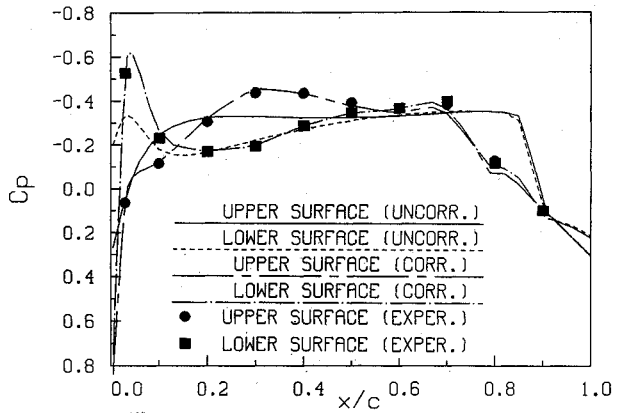

Fig. 14 Mean pressure distribution about the F-5 wing (99% span, 20 Hz).

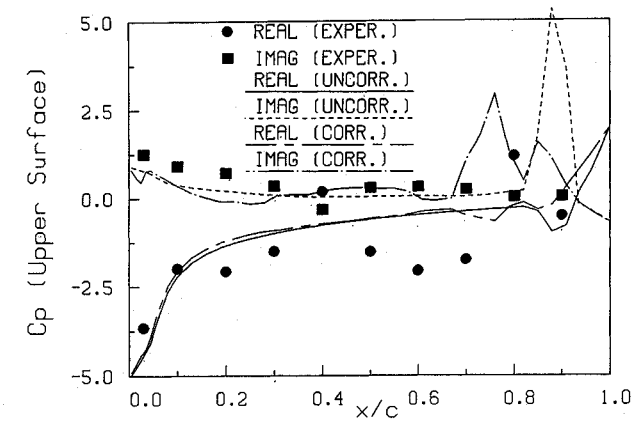

Fig. 15 Upper-surface unsteady pressure distribution about the F-5 wing (99% span, 20 Hz).

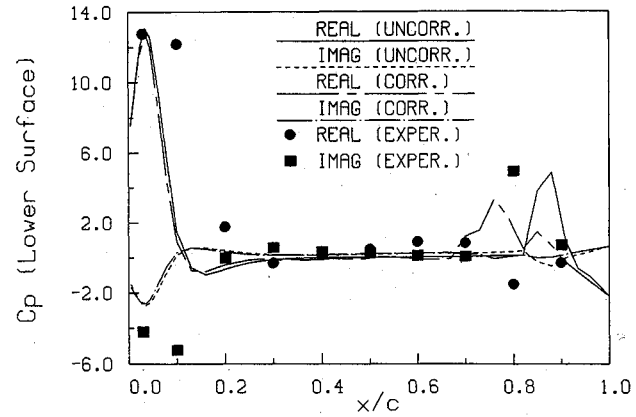

Fig. 16 Lower-surface unsteady pressure distribution about the F-5 wing (99% span, 20 Hz).

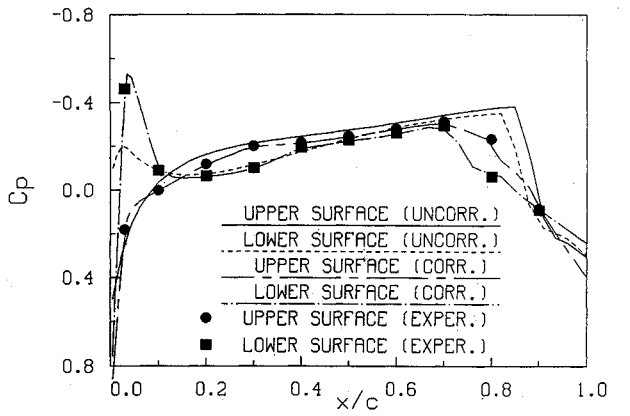

Fig. 17 Mean pressure distribution about the F-5 wing (34% span, 40 Hz).

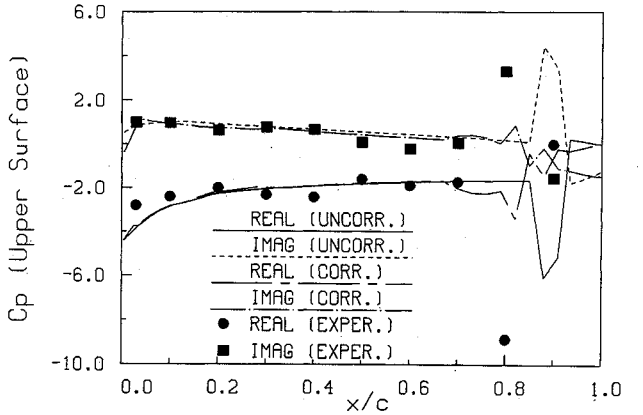

Fig. 18 Upper-surface unsteady pressure distribution about the F-5 wing (34% span, 40 Hz).

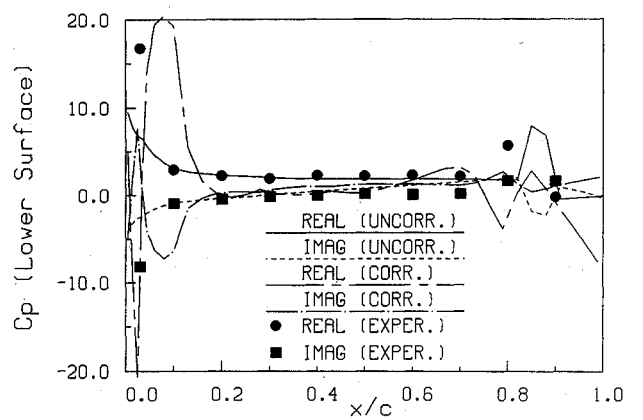

Fig. 19 Lower-surface unsteady pressure distribution about the F-5 wing (34% span, 40 Hz).

In the unsteady results, the correction also moved the trailing-edge shock forward on both surfaces and increased the magnitude of the lower surface leading-edge shock. The correction had the disadvantage of creating oscillations in the numerical results, especially on the lower surface. This might be attributed to scatter in the mean experimental data (the unsteady experimental data were not used in the correction), or the interpolation methods used.

The sparseness of the unsteady experimental data makes comparison difficult with the corrected numerical results, as the shock waves were not adequately resolved experimentally. It would thus be necessary to perform additional investigations to resolve the inaccuracies in the numerical technique.

Conclusions

Transonic small-disturbance calculations tend to be inaccurate for strong shock waves. The inaccuracy is felt in the

time-mean solution, and the unsteady fluctuation about the mean is assumed to be more accurate. A correction was applied to the unsteady pressure output from both two- and three-dimensional TSD calculations. The pressures were corrected using experimental steady-state values, and the result was a numerical time-accurate fluctuation about an experimental steady state.

The strained coordinate technique was used to transform the flowfield into a coordinate system where the shock location remains fixed. This essentially removed the nonlinearities from the flowfield solution, allowing superposition to be used to apply the pressure correction.

The results demonstrated that the pressure correction was easy to apply as a postprocessor to the output of a TSD calculation. Only steady-state experimental data were required. The correction succeeded in moving the numerical shock location closer to the experimental location. The best results occurred when there was a large error in the original shock location. A slight waviness in the corrected solution appears to be caused by scatter in the experimental data used in the correction. Another source of error is in the interpolation between sparse experimental data points. A more accurate method of interpolation between data points would lead to better resolution of the flow, especially at the leading edge and at shock locations.

Acknowledgment

This work was sponsored by Air Force Wright Aeronautical Laboratories under Contract F33615-87-C-3211.

References

[1]Ballhaus, W. F. and Bailey, F. R., "Numerical Calculation of Transonic Flow About Swept Wings," AIAA Paper 72-677, June 1972.

[2]Lomax, H., Bailey, F. R., and Balhaus, W. F., "On the Numerical Simulation of Three-Dimensional Transonic Flow with Application to the C-141 Wing," NASA TN-D-6933, Aug. 1973.

[3]Ballhaus, W. F. and Goorjian, P. M., "Implicit Finite-Difference Computations of Unsteady Transonic Flows about Airfoils," *AIAA Journal,* Vol. 15, Dec. 1977, pp. 1728–1735.

[4]Borland, C. J., Rizzeta, D. P., and Yoshihara, H., "Numerical Solution of Three-Dimensional Unsteady Transonic Flow Over Swept Wings," AIAA Paper 80-1369, July 1980.

[5]Volpe, G. and Melnik, R. E., "The Design of Transonic Airfoils by a Well-Posed Inverse Method," presented at International Conference on Inverse Design Concepts in Engineering Sciences, Dept. of Aerospace Engineering and Engineering Mechanics, Univ. of Texas at Austin, TX, Oct. 1984.

[6]Nixon, D., "Perturbation of a Discontinuous Transonic Flow," *AIAA Journal,* Vol. 16, Jan. 1978, pp. 47–52.

[7]Nixon, D., "Perturbation in Two- and Three-Dimensional Transonic Flow," *AIAA Journal,* Vol. 16, July 1978, pp. 699–709.

[8]Nixon, D. and McIntosh, S. C., "Further Observations on the Strained Coordinate Method for Transonic Flow," *AIAA Journal,* Vol. 18, Dec. 1980, pp. 1540–1541.

[9]Davis, S. and Malcolm, G., "Experimental Unsteady Aerodynamics of Conventional and Supercritical Airfoils," NASA TM-81221, Aug. 1980.

[10]Tijdeman, H. and Schippers, P., "Results of Pressure Measurements on an Airfoil with Oscillating Flap in Two-Dimensional High Subsonic and Transonic Flow (Zero Incidence and Zero Mean Flap Position)," National Aerospace Lab., The Netherlands, NLR TR-73078 U, 1973.

[11]"Compendium of Unsteady Aerodynamic Measurements," AGARD R-702, Aug. 1972.

[12]Tijdeman, H., et al., "Transonic Wind Tunnel Tests on an Oscillating Wing with External Stores; Part II. The Clean Wing," National Aerospace Lab., The Netherlands, Air Force Flight Dynamics Lab., TR-78-194, March 1979.